



# Effects of channel geometry and physicochemical properties of solutions on stable double emulsion production in planar microfluidic devices having triangular orifices

Hidema, Ruri  
Ohashi, Ryotaro  
Muller, Susan J.  
Suzuki, Hiroshi

---

**(Citation)**

AIP Advances, 11(6):065219

**(Issue Date)**

2021-06-01

**(Resource Type)**

journal article

**(Version)**

Version of Record

**(Rights)**

© 2021 Author(s).

All article content, except where otherwise noted, is licensed under a Creative Commons Attribution (CC BY) license (<http://creativecommons.org/licenses/by/4.0/>).

**(URL)**

<https://hdl.handle.net/20.500.14094/90008689>



# Effects of channel geometry and physicochemical properties of solutions on stable double emulsion production in planar microfluidic devices having triangular orifices

Cite as: AIP Advances 11, 065219 (2021); <https://doi.org/10.1063/5.0055436>

Submitted: 29 April 2021 • Accepted: 27 May 2021 • Published Online: 11 June 2021

 Ruri Hidema, Ryotaro Ohashi, Susan J. Muller, et al.



View Online



Export Citation



CrossMark

## ARTICLES YOU MAY BE INTERESTED IN

[Formation of dispersions using “flow focusing” in microchannels](#)


Applied Physics Letters **82**, 364 (2003); <https://doi.org/10.1063/1.1537519>

[Droplet formation in a T-shaped microfluidic junction](#)

Journal of Applied Physics **106**, 034906 (2009); <https://doi.org/10.1063/1.3187831>

[Microscale tipstreaming in a microfluidic flow focusing device](#)

Physics of Fluids **18**, 121512 (2006); <https://doi.org/10.1063/1.2397023>



# Effects of channel geometry and physicochemical properties of solutions on stable double emulsion production in planar microfluidic devices having triangular orifices

Cite as: AIP Advances 11, 065219 (2021); doi: 10.1063/5.0055436

Submitted: 29 April 2021 • Accepted: 27 May 2021 •

Published Online: 11 June 2021



Ruri Hidema,<sup>1,a)</sup>  Ryotaro Ohashi,<sup>1</sup> Susan J. Muller,<sup>2</sup> and Hiroshi Suzuki<sup>1</sup> 

## AFFILIATIONS

<sup>1</sup> Department of Chemical Science and Engineering, Kobe University, Kobe 657-8501, Japan

<sup>2</sup> Department of Chemical and Biomolecular Engineering, University of California, Berkeley, Berkeley, California 94720, USA

<sup>a)</sup> Author to whom correspondence should be addressed: [hidema@port.kobe-u.ac.jp](mailto:hidema@port.kobe-u.ac.jp). Telephone: +81-78-803-6657.

Fax: +81-78-803-6657

## ABSTRACT

The planar microfluidic devices for producing double emulsions are beneficial in terms of accuracy and facility in fabrication. However, factors such as the flow rates, interfacial tensions, viscosities, channel geometry, and wettability of the devices affect the stability of the double emulsion production. In this study, we have focused on double emulsion production in a planar flow focusing device with triangle-shaped orifices. The local velocity in the channel can be controlled by modifying the channel design. Here, we have used two types of microfluidic devices with orifices and junctions of different shapes, denoted as mc-A and mc-B. By controlling the orifice angles and the width of the junctions, the stable flow regimes characterized in a capillary number space were expanded, and the production efficiency was increased. The effects of interfacial tensions of the sample solutions on the stability of double emulsion production were also examined. The double emulsions produced under stable conditions were highly uniform, and the diameter of the produced emulsions was well defined by the capillary numbers. However, the diameter of the double emulsions was mainly affected by the size of the orifice.

© 2021 Author(s). All article content, except where otherwise noted, is licensed under a Creative Commons Attribution (CC BY) license (<http://creativecommons.org/licenses/by/4.0/>). <https://doi.org/10.1063/5.0055436>

## I. INTRODUCTION

The processes of production and manipulation of droplets in microscale devices have attracted considerable research attention in the last two decades. Microfluidic droplet formation has been intensively studied and shows potential for future applications, such as in chemical reactions in a confined space, particle production, synthesis of cell-like biomaterials, and encapsulation of biological molecules or drugs.<sup>1–9</sup> An important aspect to ensure for achieving uniform and stable droplets in droplet formation processes is the control of the fluid interface. In particular, at the microscale, the interfaces of immiscible fluids play a key role. To exploit the advantages of microscale processes, several types of microfluidic devices and techniques have been proposed previously.<sup>4</sup>

Flow focusing is a widespread microfluidic method for producing uniform droplets. There are two primary approaches as part of this method.<sup>10</sup> One is geometrical flow focusing; here, fluids are injected into a device having orifices with a size smaller than the channel width.<sup>11</sup> The other is hydrodynamic flow focusing; in this case, the fluids meet at a cross-junction to produce droplets as a result of interface instabilities.<sup>12,13</sup> Flow focusing is a promising technique for producing uniform droplets when the flow is stable and well-controlled. However, flow regimes in a device are affected by several factors, such as channel geometry, flow rates, viscosity, and interfacial tension. A trivial factor easily destabilizes the fluid interface, which prohibits the production of uniform droplets.

To quantify the flow regimes in the droplet formation process, immiscible liquid–liquid systems that produce emulsions<sup>11,12,14–16</sup>

and gas–liquid systems that produce bubbles<sup>17–19</sup> have been studied in several types of geometrical flow focusing devices. In this regard, a pioneering study on geometrical flow focusing was conducted by Anna *et al.*<sup>11</sup> Moreover, a series of experimental studies have yielded observations on the formation of liquid drops in the continuous phase of a second immiscible fluid using a planar flow focusing device.<sup>11,14,16</sup> Droplet breakup processes, droplet sizes, characteristic droplet formation times, and thread formation before droplet breakup were investigated in these studies. In microfluidic flows, the Reynolds number is very small and the inertia can thus be neglected. Therefore, the capillary number  $Ca$ , which quantifies the balance of viscous drag forces and capillary pressure, is an appropriate dimensionless number for describing the droplet breakup processes. Lee *et al.*<sup>16</sup> proposed  $Ca$  that contains all the geometric dimensions that are defined in terms of the effective rate of strain in a contraction region. The proposed  $Ca$  well described the effects of channel geometry, flow rates, viscosity ratio, and interfacial tension on the droplet formation process and flow regimes. Planar rectangular devices that have similar geometry as that of the devices proposed by Anna *et al.*<sup>11</sup> have often been used to clarify the pinch-off process in two-phase flow.<sup>15,18,20,21</sup> A device with a triangle-shaped orifice was also tested to produce droplets; specifically, the velocity and pressure fields in the device were simulated.<sup>22,23</sup>

Hydrodynamic flow focusing has usually been studied in devices having a simple cross-channel junction. Cubaud and Mason studied liquid–liquid systems in devices with cross-channel junctions and observed the flow regimes of the inner fluids.<sup>12</sup> The flow regimes were categorized as threading, jetting, dripping, tubing, and displacement, and the characteristic parameters of these regimes were quantified by the flow rates, viscosities, interfacial tension, capillary number of fluids, and channel geometry.<sup>12</sup> The pinch-off process and instability of the inner liquid phase in a hydrodynamic flow focusing device were also studied, and it was shown that the geometric confinement of the inner liquid phase in microfluidic devices affects drop formation.<sup>24,25</sup> To highlight the droplet formation process in the devices, the particle image velocimetry (PIV) was used to measure the velocity profiles around the droplet in the pinch-off process.<sup>24,26,27</sup> The round shape of a flow focusing junction and the angle of the cross-junction have also been observed to affect the pinch-off process and droplet size.<sup>28–30</sup>

As introduced in the above paragraphs, the factors that stabilize and control emulsion or bubble production in a two-phase flow are relatively limited and well-identified. Conversely, the production of double- or multi-layered emulsions in three-phase or multiphase flows is more complex. Therefore, several types of microfluidic devices have been proposed; these devices are mainly categorized in planar micro-channel and micro-capillary devices.<sup>4,31–33</sup> Unlike micro-capillary devices, it is possible to fabricate channels with a variety of designs and to control the design precisely in a double emulsion production based on a planar microchannel.<sup>34,35</sup> A precisely controlled channel is required to produce desirable double emulsions. However, for a planar microchannel, the flow rates, interfacial tensions, and viscosity ratios of several fluids, channel geometry, and wettability of the devices all affect the stability of double emulsion production. The flow is easily converted to an unstable flow regime, which leads to a failure of the double emulsion production in a planar microchannel. Therefore, many studies have previously discussed double emulsion production in several types of

planar microfluidic devices. Nie *et al.*<sup>36</sup> and Seo *et al.*<sup>37</sup> proposed a planar microfluidic flow focusing device with a contraction part. Abate *et al.*<sup>38,39</sup> proposed a flow focusing device with two cross-junctions, and a planar microfluidic device with a triangle-shaped orifice was also proposed.<sup>40,41</sup> For all the cases, the flow rates, interfacial tensions, and the wettability of the device had a considerable impact on the flow regimes. In particular, the wettability of the device is a critical factor that significantly influences the double emulsion production.<sup>37,38,40–42</sup>

To quantify empirical knowledge obtained by experimental works, numerical studies have also been conducted, which characterize the flow regimes in various types of devices.<sup>43–50</sup> Jensen *et al.*<sup>43</sup> and Zhou *et al.*<sup>44</sup> conducted a numerical study on emulsions and double emulsions in a planar microfluidic device similar to that of Anna *et al.*<sup>11</sup> Recently, the dripping and jetting processes as part of double emulsion formation in the capillary device have been numerically evaluated,<sup>45,46</sup> as have one-step and two-step processes in devices with two cross-junctions.<sup>47,48</sup> The flow regimes of double emulsion formation have been categorized as a function of  $Ca$ .<sup>48,51</sup> However, as revealed by Wang *et al.*,<sup>48</sup> a stable formation region on the  $Ca$  space is limited. This suggests that a slight change in each factor affects the stability of the double emulsion formation.

In this study, we have focused on double emulsion production in a planar flow focusing device with triangle-shaped orifices. Although several previous studies have discussed double emulsion production in several types of planar microfluidic devices, a common understanding of the production of stable double emulsions has not been completely obtained. In particular, there are few discussions on characterizing flow regimes and optimizing devices in the case of triangular orifices. The advantages of the triangular orifices are that the local velocities in the channel are controlled by modifying the size of the small slit of the orifices and the angle of the triangular orifices. Capabilities to control the local velocity with the triangular orifices are expanded compared to a common flow focusing device with a cross-junction where the local velocities in the channel are controlled by only the flow rates. Controlling the local velocities in the device can help stabilize the flow regimes, lead the efficient pinch-off process, and control the production rate. Therefore, the purpose of this study was to characterize the flow regimes of double emulsion production in several planar microfluidic devices with triangle-shaped orifices and to clarify the effects of the orifices on the stability of double emulsion production and production efficiency. The shape of the orifices and solution properties were varied to consider their effects on the size of the double emulsions and on the stability of the production.

In Secs. II–IV, we first describe the experimental conditions and the two microfluidic device types. Furthermore, we present the definition of the capillary number that has been used in this study and characterize the flow regimes based on the capillary number. Subsequently, the size variation of the produced double emulsion was discussed based on the capillary number. Finally, we compared the stability and production rates in both channels.

## II. EXPERIMENTAL PROCEDURES

### A. Materials

To produce a water-in-oil-in-water (W/O/W) double emulsion, an internal aqueous solution, a lipid oil-phase solution, and



an external aqueous solution were prepared. The internal aqueous solution contained surfactants of 0.025 wt. % Pluronic F68 [polyoxyethylene polypropylene glycol (160E.O.) (30P.O.), FUJIFILM Wako Pure Chemical Corporation] in ultrapure water, and the solution is denoted by  $w_{in}$ . The lipid oil-phase solution contained lipids of 6.5 mM DOPC (COATSOME, 1,2-dioleoyl-sn-glycero-3-phosphocholine, NOF Corporation.) dissolved in oleic acid, denoted as  $o_{lip}$ . Moreover, two solutions containing different concentrations of the surfactant were prepared as external aqueous solutions. The original external aqueous solution was composed of 2.85 vol. % of 10 wt. % Pluronic F68 solution, 14 vol. % of glycerol (FUJIFILM Wako Pure Chemical Corporation), 14 vol. % of ethanol (FUJIFILM Wako Pure Chemical Corporation), and deionized pure water; the solution is denoted by  $w_{ex1}$ . The other external aqueous solution contained 8.55 vol. % of 10 wt. % Pluronic F68 solution. The concentration of Pluronic F68 in the solution is three times greater than that of  $w_{ex1}$ ; thus, this solution is denoted as  $w_{ex3}$ . A fluorescent probe DiI-C18 (1,1'-dilinoleyl-3,3,3',3'-tetramethylindocarbocyanine perchlorate, Life Technologies Corporation) was added to the lipid solution for fluorescence microscopy imaging. The physical parameters of all fluids used in the experiment are listed in Tables I–III.

## B. Microfluidic device fabrication and surface treatment

The microfluidic devices were fabricated in polydimethylsiloxane (PDMS) using conventional soft lithography techniques. A 4-in. silicon wafer was spin-coated with a layer of SU-8 3050 (Nippon Kayaku Co., Ltd.) photoresist; the spin speed was fixed at 500 rpm for 10 s, followed by a speed of 2200 rpm for 30 s. Subsequently, the wafer was baked on a hotplate at 65 °C for 1 h and then at 90 °C for 10 min to improve the adhesion of SU-8 to the silicon wafer. The device designs were then patterned on the wafer via exposure to UV light through a high-resolution photomask containing the channel design. The wafer was baked at 65 °C for

**TABLE I.** Viscosity of each sample solution.  $\eta$  denotes the viscosity, and each subscript notation denotes each sample solution.

$\eta_{w_{in}}$ (Pa s)	$\eta_{o_{lip}}$ (Pa s)	$\eta_{w_{ex1}}$ (Pa s)	$\eta_{w_{ex3}}$ (Pa s)
$0.886 \times 10^{-3}$	$29.8 \times 10^{-3}$	$2.25 \times 10^{-3}$	$1.58 \times 10^{-3}$

**TABLE II.** Density of each sample solution.  $\rho$  denotes the density, and each subscript notation denotes each sample solution.

$\rho_{w_{in}}$ (kg/m <sup>3</sup> )	$\rho_{o_{lip}}$ (kg/m <sup>3</sup> )	$\rho_{w_{ex1}}$ (kg/m <sup>3</sup> )	$\rho_{w_{ex3}}$ (kg/m <sup>3</sup> )
1000	896	1005	1005

**TABLE III.** Interfacial tension at the interface between each liquid-phase and lipid oil-phase solution.  $\gamma$  denotes the interfacial tension, and each subscript notation denotes the interface between the two sample solutions.

$\gamma_{o_{lip}/w_{in}}$ (mN/m)	$\gamma_{o_{lip}/w_{ex1}}$ (mN/m)	$\gamma_{o_{lip}/w_{ex3}}$ (mN/m)
5.1	1.4	0.9

1 min and then at 90 °C for 4 min for post-exposure baking. After post-exposure baking, the wafer was immersed in a SU-8 developer (MICRO CHEM) with shaking for 5 min to form the channel design. The wafer was baked at 150 °C for 1 h, after which the surface was spin-coated with 1,1,1,3,3,3-hexamethyldisilazane (FUJIFILM Wako Pure Chemical Corporation) for finishing. The SU-8 pattern on the wafer was a positive mold for the PDMS. The height of the mold was measured using Dektak XT-A (Bruker Corporation), which was ~50  $\mu$ m. The PDMS (SYLGARD™ 184 Silicone Elastomer Base, Dow Chemical Company) was mixed with the silicone elastomer curing agent in a 10:1 ratio. After the PDMS mixture was degassed in vacuum, it was poured on the mold wafer and then baked at 60 °C for 4 h. Subsequently, the PDMS was peeled off the mold, cut into individual devices, pierced holes with needles, and cleaned. The device was bonded to a cleaned glass slide after plasma treatment, which was baked at 60 °C for 30 min and then rested overnight.

Hydrophilic treatment was applied to the outermost channel: 1 wt. % aqueous solution of polyvinyl alcohol [PVA, poly (vinyl alcohol) 1000, completely hydrolyzed, with an average degree of polymerization of ~900 to 1100, FUJIFILM Wako Pure Chemical Corporation] was injected into the outermost channel and rested for 10 min. The PVA solution was then withdrawn using a needle and baked for 10 min. The injection and removal of the PVA solution and subsequent baking process were repeated three times. The hydrophilicity of the outermost channel and the second orifice—as shown in Fig. 1 and explained in the following paragraph—are very important to ensure to avoid oil contamination; that is, the lipid oil-phase solution is not pinched-off at the orifice and spread in the reservoir. This clearly leads to failure of double emulsion production. After the process, the outermost channel and the second orifice were observed by a microscope to eliminate the channel that is blocked by excess treatment of PVA.

Herein, we prepared two types of channel designs based on a previous study,<sup>40</sup> as shown in Fig. 1. Each device was named micro-channel A (mc-A) and micro-channel B (mc-B). Both devices had three inlets, one outlet, and two triangular orifices. The differences between the devices were in the design of the two orifices. The angle  $\alpha$  at the first orifice (OR1) of mc-A was larger than that of mc-B. Although the angle  $\beta$  at the second orifice (OR2) was the same for both channels, angle  $\gamma_3$  was different for both channels. The detailed scale of the devices is listed in Table IV. To achieve stable double emulsion production in a wide range of experimental parameters and to increase the production rate, the angles of the two orifices in the device were verified; mc-B had a sharper angle at OR1 to increase the production rate by prohibiting deceleration at the orifice, and it had a wide junction before OR2 to increase stability. The wide junction increased the contact area between two immiscible fluids, which stabilized the pinch-off process prohibiting, for example, the threading flow regime and oil contamination at the orifice.

## C. Double emulsion production and observation of flow regimes

The entire image of the device is shown in Fig. 1(a). The device had three inlets for each solution. Each inlet was connected to a syringe via tubing and filled with each solution. The internal aqueous solution,  $w_{in}$ , the lipid oil-phase solution,  $o_{lip}$ , and the external

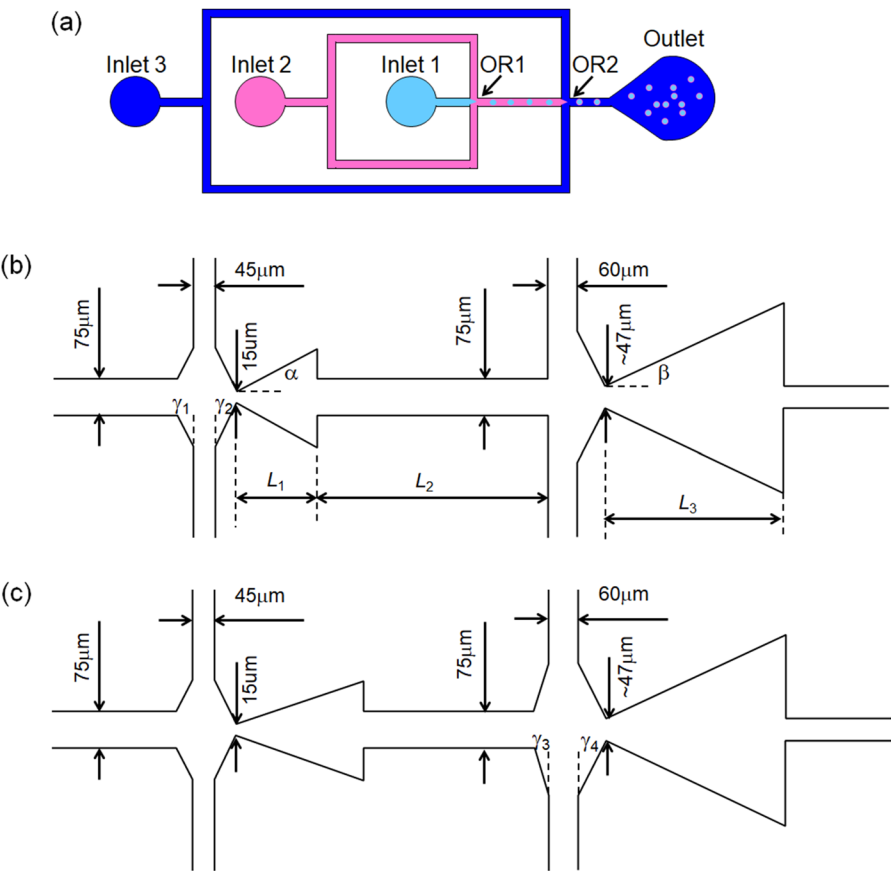


**FIG. 1.** Schematics of planar microchannels (a) with detailed scales of orifices in mc-A (b) and mc-B (c).  $\alpha$  (deg) and  $\beta$  (deg) are the angles at the first and the second orifice as indicated in (b).  $\gamma_1$  (deg),  $\gamma_2$  (deg),  $\gamma_3$  (deg), and  $\gamma_4$  (deg) are the angles at the intersections before each orifice as indicated in (b) and (c).  $L_1$  ( $\mu\text{m}$ ),  $L_2$  ( $\mu\text{m}$ ), and  $L_3$  ( $\mu\text{m}$ ) are the length of each position as indicated in (b). The channels are line-symmetric. The value of each geometric parameter is shown in Table IV.

**TABLE IV.** Geometric parameters of the channels.

	$\alpha$ (deg)	$\beta$ (deg)	$\gamma_1$ (deg)	$\gamma_2$ (deg)	$\gamma_3$ (deg)	$\gamma_4$ (deg)	$L_1$ ( $\mu\text{m}$ )	$L_2$ ( $\mu\text{m}$ )	$L_3$ ( $\mu\text{m}$ )
mc-A	16	17	32	32	0	12	304	8711	954
mc-B	9	17	32	32	9	12	609	8366	954

aqueous solution,  $w_{\text{ex1}}$  or  $w_{\text{ex3}}$ , were injected into the device from inlets 1, 2, and 3, respectively. The flow rates were controlled using syringe pumps (Harvard Apparatus). The flow rates of the internal aqueous solution,  $Q_{\text{win}}$  ( $\mu\text{l/h}$ ), the lipid oil-phase solution,  $Q_{\text{olip}}$  ( $\mu\text{l/h}$ ), and the external solution,  $Q_{\text{wex1}}$  or  $Q_{\text{wex3}}$  ( $\mu\text{l/h}$ ), are listed in Table V. The OR1 in the device produced “water-in-oil” emulsions, and the OR2 in the device produced “water-in-oil-in-water” double emulsions, which were carried to the reservoir. The double emulsions were visualized under a microscope (Olympus, IX83) by bright-field or fluorescent observation. Fluorescent molecules were dissolved in the lipid solution to visualize the oil phase and shell thickness of the double emulsion. The flow was recorded using a high-speed video camera (IDT Japan, Inc., Os8-S1) at 500–2000 fps.

The flow regimes at OR2 were categorized into four main types: squeezing, dripping, jetting, and threading (Fig. 2). The squeezing and dripping flow regimes are defined based on the inner droplet size. In the squeezing flow regime, the inner droplet size is larger

than the width of the second orifice. Thus, the inner droplets block the second orifice when passing through the orifice [Fig. 2(a)]. In the dripping flow regime, the inner droplet size is smaller than the width of the second orifice [Fig. 2(b)]. The flow rate ratio of the discrete phase to the continuous phase defined the flow mode as the squeezing or the dripping. The jetting flow regime where the double emulsion is pinched off at the downstream of the orifice is occurred by increasing the flow rate of the external aqueous phase [Fig. 2(c)]. The threading flow regime occurs when the flow rate of the external aqueous phase is low, which does not

**TABLE V.** Flow rates of each sample solution.  $Q$  denotes the density, and each subscript notation denotes each sample solution.

$Q_{\text{win}}$ ( $\mu\text{l/h}$ )	$Q_{\text{olip}}$ ( $\mu\text{l/h}$ )	$Q_{\text{wex1}}$ or $Q_{\text{wex3}}$ ( $\mu\text{l/h}$ )
50	50–200	100–3000

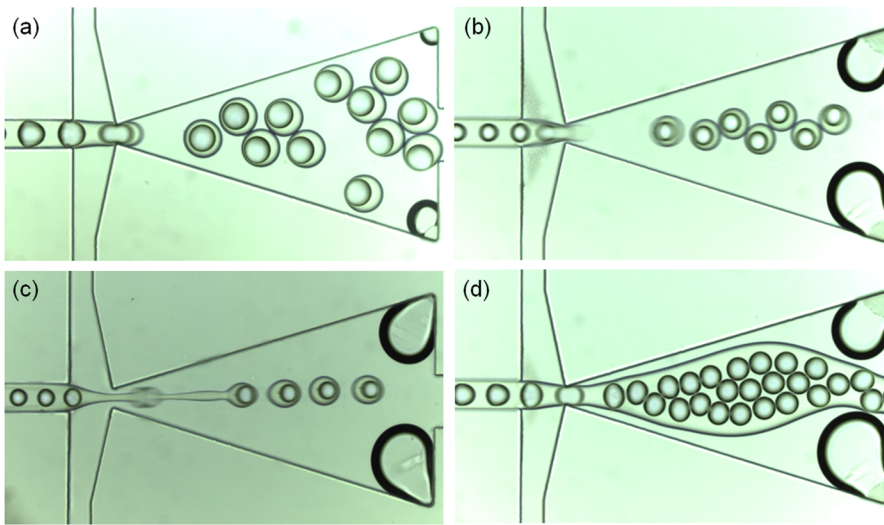


**FIG. 2.** Flow regimes categorized into four main types as (a) squeezing, (b) dripping, (c) jetting, and (d) threading.

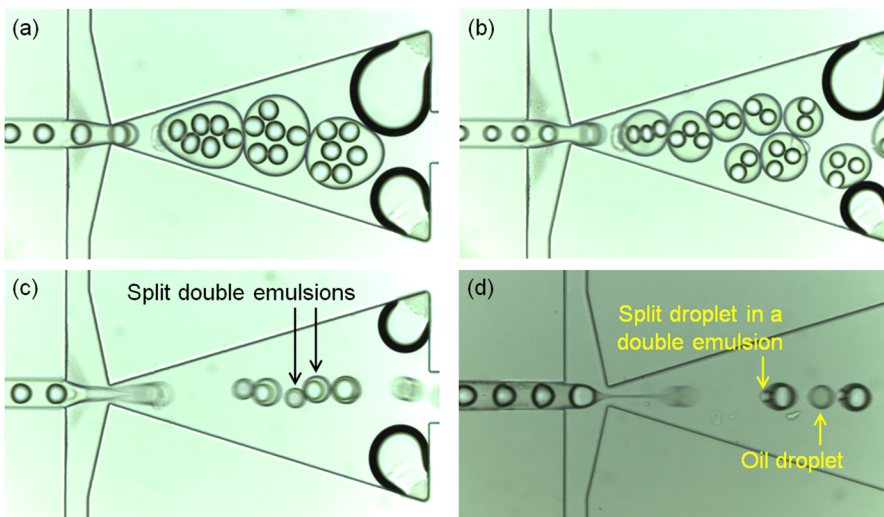


**FIG. 3.** Subcategories for describing unstable flow regimes. (a) and (b) Multiple emulsions are encapsulated in a double emulsion, which is categorized as "multiple-in-1." (c) A double emulsion is split into two double emulsion, which is categorized as "split." (d) A double emulsion is split into an oil droplet and a double emulsion, which is categorized as "oil-droplet."

produce double emulsions [Fig. 2(d)]. Several subcategories were branched from the main flow regimes, based on the number of water droplets in a single double emulsion and the stability to produce a uniform double emulsion. A double emulsion containing a single water droplet is denoted as "1-in-1," and a double emulsion containing two water droplets is denoted as "2-in-1" "3-in-1"; multiple droplets encapsulated in a double emulsion, denoted as "Multi-in-1," were also produced depending on the stability of the flow. The internal aqueous phase and the lipid oil phase could be separated into two parts: The former is denoted as "split," and the latter is denoted as "oil-droplet." Each flow regime is summarized in Fig. 3, which was used to quantify the stability of the double emulsion production.

### III. RESULTS AND DISCUSSION

#### A. Flow regime diagrams

To clarify the stability of double emulsion production in the microfluidic devices, the flow regimes at OR2 in each device were characterized as a function of capillary number ( $Ca$ ).  $Ca$  was calculated based on the physical properties of each solution at OR2, as shown in the following equations ( $Ca$  represents the magnitude of the effects of the viscous drag force due to the continuous phase on the discrete phase to the interfacial tension between these two fluids):

$$Ca(w_{in} + o_{lip}) = \frac{\eta_{oil} V(w_{in} + o_{lip})}{\gamma_{oil/wex}}, \quad (1)$$

$$Ca(w_{ex}) = \frac{\eta_{w_{ex}} V(w_{ex})}{\gamma_{o_{lip}/w_{ex}}}. \quad (2)$$

Here,  $\eta_{o_{lip}}$  (Pa s) is the viscosity of the lipid oil-phase solution, and  $V(w_{in} + o_{lip})$  is the mean velocity at OR2 calculated by the cross-sectional area of OR2 and the total flow rate of  $Q_{w_{in}}$  and  $Q_{o_{lip}}$ .  $\gamma_{o_{lip}/w_{ex}}$  is the interfacial tension between the external aqueous solution  $w_{ex1}$ ,  $w_{ex3}$ , and the lipid oil-phase solution,  $o_{lip}$ . Thus,  $Ca(w_{in} + o_{lip})$  is calculated using each parameter based on the discrete phase at OR2. Similarly,  $\eta_{w_{ex}}$  (Pa s) is the viscosity of  $w_{ex1}$  or  $w_{ex3}$ , and  $V(w_{ex})$  is the mean velocity of each external aqueous solution.  $Ca(w_{ex})$  is calculated using the parameters of the continuous phase.

Figure 4 shows the flow regime diagrams of double emulsion production at OR2 in mc-A as a function of  $Ca(w_{in} + o_{lip})$  and

$Ca(w_{ex})$ . The flow regimes are summarized in Figs. 2 and 3. Stable double emulsions were produced at the point denoted by “1-in-1” without any oil droplets. The 1-in-1 stable double emulsion was produced by various types of flow regimes such as squeezing, dripping, and jetting at a certain condition. The stable flow regime altered to 2-in-1, multi-in-1, “split,” and “oil-droplet.” Figures 4(a) and 4(b) denote the variation of flow regimes producing double emulsions with  $w_{ex1}$  or  $w_{ex3}$ . In Fig. 4, increasing the flow rates of the discrete phase and the continuous phase corresponded to increasing each capillary number  $Ca(w_{in} + o_{lip})$  and  $Ca(w_{ex1})$  or  $Ca(w_{ex3})$ . The threading region appeared when the flow rates of the continuous phase were low where  $Ca(w_{ex1})$  or  $Ca(w_{ex3})$  was low, and the flow rates of the discrete phase were high where  $Ca(w_{in} + o_{lip})$  was high. The flow regime varied from threading to squeezing, dripping, and jetting by increasing the capillary number calculated by the

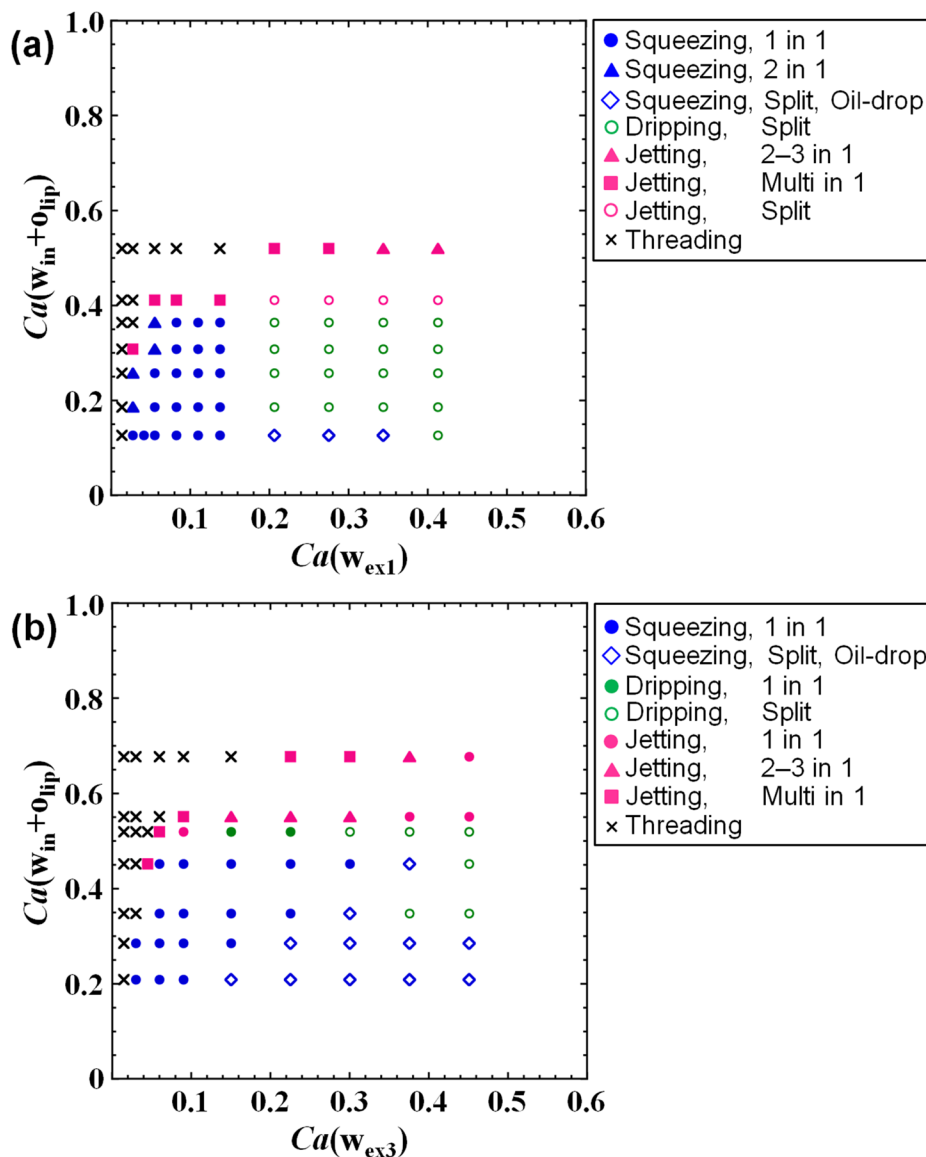


FIG. 4. Flow regime diagrams of double emulsion production at OR2 in mc-A on a  $Ca(w_{in} + o_{lip})$  and  $Ca(w_{ex})$  space. The external aqueous solutions are (a)  $w_{ex1}$  and (b)  $w_{ex3}$ .

parameter of continuous phase as  $Ca(w_{ex1})$  or  $Ca(w_{ex3})$ . The interface tension  $\gamma_{oil/w_{ex3}}$  was lower than  $\gamma_{oil/w_{ex1}}$ , which stabilized the interface between  $w_{ex3}$  and  $oil$ . Therefore,  $w_{ex3}$  expanded the stable flow region producing 1-in-1 double emulsions on the  $Ca$  mapping [Fig. 4(b)].

Figure 5 shows the flow regimes in mc-B, which had a wider cross-junction at OR2. The wide cross-junction increased the interface area between  $w_{ex}$  and  $oil$  at OR2 when the external aqueous solution covered the lipid oil-phase solution to pinch-off. This stabilized the pinch-off process; therefore, the stable flow region producing 1-in-1 double emulsions expanded on the  $Ca$  mapping of mc-B. In addition to mc-A,  $w_{ex3}$  also expanded the stable flow region in mc-B.

### B. Scaling analysis of the sizes of stable double emulsions

Double emulsions produced under stable conditions were uniform and size-controlled, as shown in Figs. 6 and 7. The particle size

was quantified by the mean diameter, while the polydispersity of the system was quantified using the coefficient of variation (CV). CV is the ratio of the standard deviation to mean diameter; CV of the stable double emulsions produced in both mc-A and mc-B was as low as 1%–2%.

The evolution of the internal diameter of a double emulsion,  $D_{in}$  ( $\mu m$ ), in both mc-A and mc-B as a function of  $Q_{oil}/Q_{win}$  is presented in Fig. 8. Although  $Q_{win}$ ,  $Q_{oil}$ ,  $Q_{w_{ex1}}$ , and  $Q_{w_{ex3}}$  varied over a wide range, as indicated in Table V, only the cases that produced stable 1-in-1 double emulsions are plotted in Fig. 8.  $D_{in}$  of the double emulsion produced in both channels is plotted on a logarithmic scale arranged linearly, which is described by the following equation:

$$D_{in} = A(Q_{oil}/Q_{win})^{-n}, \quad (3)$$

where  $A$  [–] is a coefficient and  $n$  [–] is an index. Here,  $n = 0.291$ . The evolution of the diameter of a double emulsion,  $D_{DE}$  ( $\mu m$ ), showed a slight decrease with  $Q(w_{ex})/Q(w_{in} + oil)$ , as shown in Eq. (4).

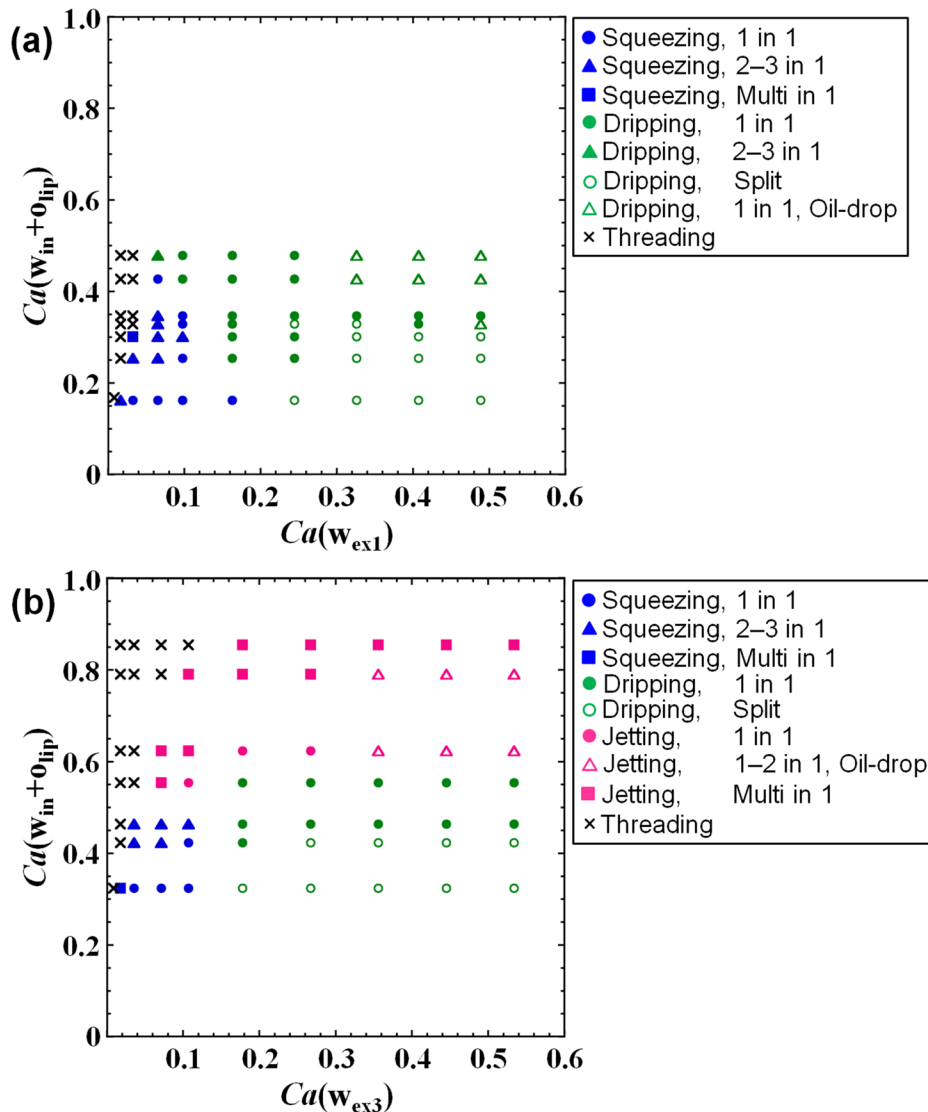


**FIG. 5.** Flow regime diagrams of double emulsion production at OR2 in mc-B on a  $Ca(w_{in} + oil)$  and  $Ca(w_{ex})$  space. The external aqueous solutions are (a)  $w_{ex1}$  and (b)  $w_{ex3}$ .



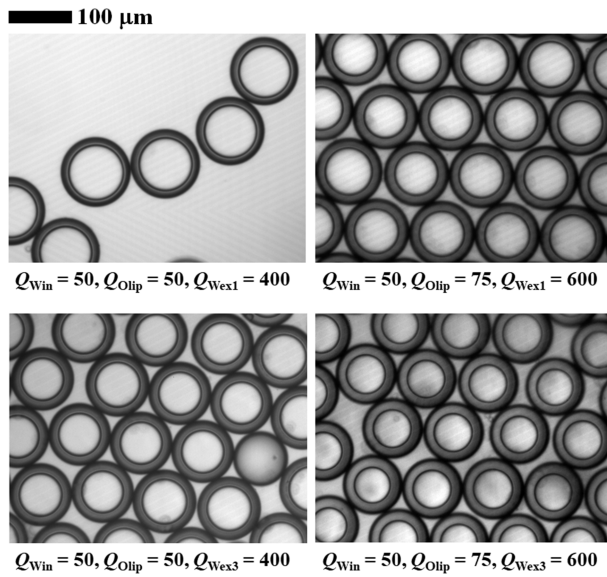


FIG. 6. Example of uniform double emulsions produced in mc-A. The flow rates that produced the double emulsions are shown.

However, the correlation was weak, as indicated by the small value of the index,  $n = 0.0628$ , as shown in Fig. 9,

$$D_{DE} = A(Q_{wex}/(Q_{win} + Q_{olip}))^{-n}. \quad (4)$$

$D_{in}$  was arranged linearly to  $Ca(o_{lip})$  and  $Ca(o_{lip})/Ca(w_{in})$ .  $Ca(o_{lip})$  and  $Ca(w_{in})$  were calculated based on the velocity of  $o_{lip}$ ,  $V(o_{lip})$ , and  $w_{in}$ ,  $V(w_{in})$ , at OR1, and the interfacial tension between them,  $\gamma_{o_{lip}/w_{in}}$ ;  $Ca(o_{lip}) = \{\eta_{o_{lip}} V(o_{lip})\}/\gamma_{o_{lip}/w_{in}}$ , and

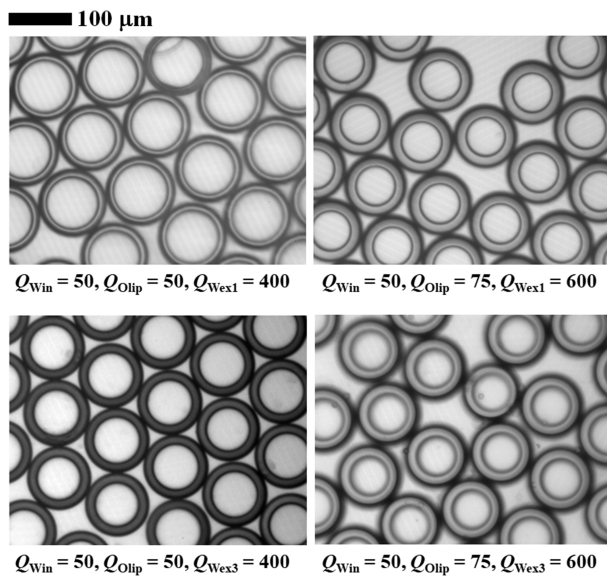


FIG. 7. Example of uniform double emulsions produced in mc-B. The flow rates that produced the double emulsions are shown.

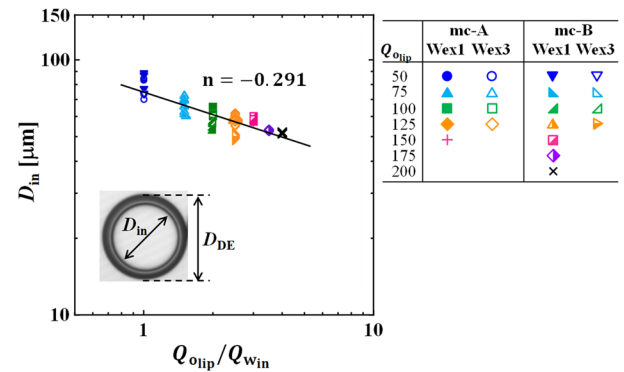


FIG. 8.  $D_{in}$  of double emulsions produced in mc-A or mc-B as a function of the flow rate ratio. The inset image indicates  $D_{in}$  and  $D_{DE}$ .

$Ca(w_{in}) = \{\eta_{w_{in}} V(w_{in})\}/\gamma_{o_{lip}/w_{in}}$ . Figures 10 and 11 show  $D_{in}$  that was decreased by increasing  $Ca(o_{lip})$  with  $n = 0.224$  and by  $Ca(o_{lip})/Ca(w_{in})$  with  $n = 0.291$  in the same manner as Eq. (3).

The indices  $n$  obtained by  $D_{DE}$  plotted against  $Ca(w_{ex})$  and  $Ca(w_{ex})/Ca(w_{in} + o_{lip})$  were 0.0820 and 0.0439, as shown in Figs. 12 and 13, respectively, which are small. These small indices obtained by  $D_{DE}$  plotted to the flow rates and capillary number indicate that the flow rates and interfacial tension hardly affected the size of the double emulsion. These small indices obtained in this study were smaller than a value reported in a previous study that uses a capillary tube with a T-shaped junction.<sup>33</sup> This indicates that the size of the double emulsion produced in mc-A and mc-B was limited by the size of the small slit of OR2. In the case of the triangle-shaped orifices, the size of the double emulsions was strongly affected by the orifice size. However, the stable flow area on a capillary number space to produce stable 1-in-1 double emulsion was expanded compared with a device with T-shaped junction or cross-junction.<sup>48</sup>

### C. Shedding frequency at each orifice to realize stable production

Figure 14 shows the shedding frequency of the emulsions at OR1 and that of the double emulsions at OR2. Stable double emulsions were produced at OR2 when the frequencies of both orifices

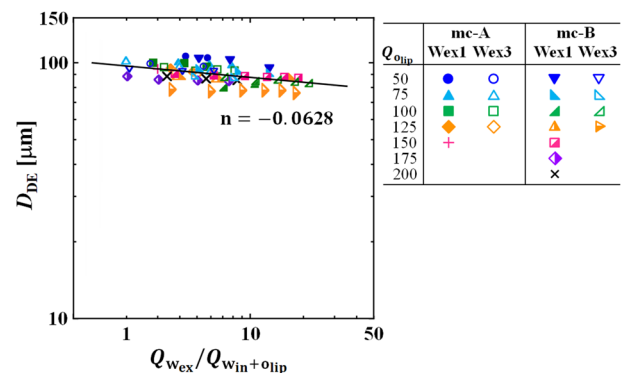


FIG. 9.  $D_{DE}$  of double emulsions produced in mc-A or mc-B as a function of the flow rate ratio.



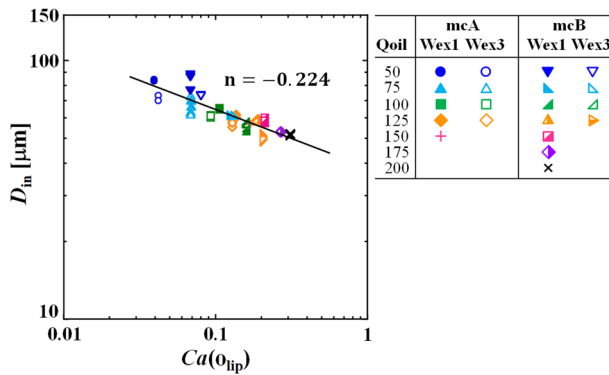


FIG. 10.  $D_{in}$  of double emulsions produced in mc-A or mc-B as a function of  $Ca(o_{lip})$ .

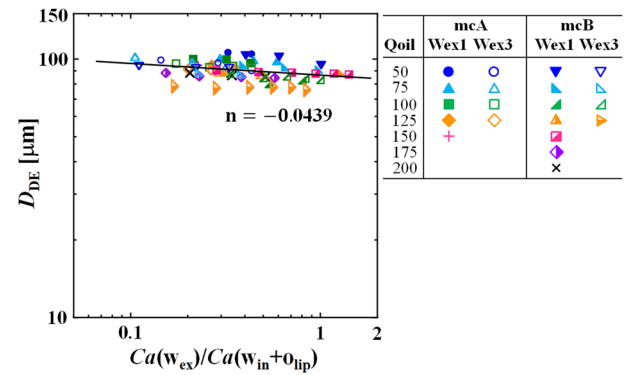


FIG. 13.  $D_{DE}$  of double emulsions produced in mc-A or mc-B as a function of  $Ca(w_{ex})/Ca(w_{in} + o_{lip})$ .

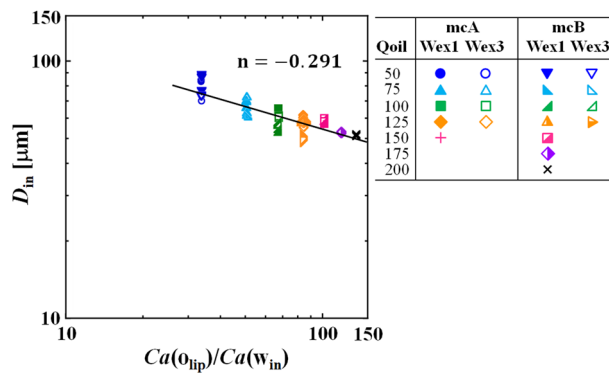


FIG. 11.  $D_{in}$  of double emulsions produced in mc-A or mc-B as a function of  $Ca(o_{lip})/Ca(w_{in})$ .

were the same. In the case of mc-A, stable double emulsions were produced when  $400 \leq Q_{w_{ex1}} \leq 1000$  and  $400 \leq Q_{w_{ex3}} \leq 1500$ . In the case of mc-B, stable double emulsions were produced over a wider range with both external solutions when  $1000 \leq Q_{w_{ex1}}, Q_{w_{ex3}} \leq 3000$ . In addition, the shedding frequency observed in mc-B was 2–3 times

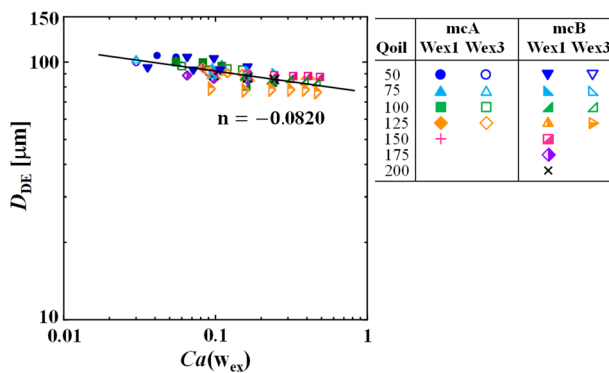


FIG. 12.  $D_{DE}$  of double emulsions produced in mc-A or mc-B as a function of  $Ca(w_{ex})$ .

larger than that in mc-A. Therefore, mc-B produced stable double emulsions with a wider range of flow rates at higher efficiency. The promising results indicate that the production stability and production rates can be controlled by modifying a design of the cross-junction and orifice angle, which affects the local velocity in the

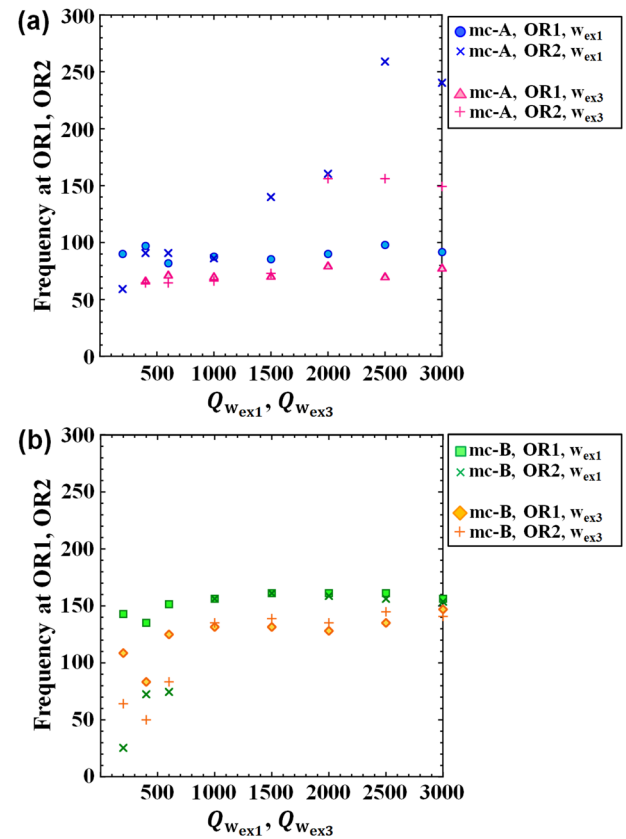


FIG. 14. Shedding frequency of emulsions at OR1 and that of double emulsions at OR2.  $Q_{w_{in}}$  and  $Q_{o_{lip}}$  were fixed at 50 and 100  $\mu\text{l/h}$ , respectively, and  $Q_{w_{ex}}$  was varied from 200 to 3000  $\mu\text{l/h}$ . Shedding frequency in (a) mc-A and (b) mc-B.

channel. Moreover, an appropriate interfacial tension stabilizes the double emulsion production;  $w_{ex3}$  expanded the stable region.

#### IV. CONCLUSION

Although many studies have previously discussed double emulsion production in several types of microfluidic devices, obtaining a common understanding on the characterization of the flow regimes has proven challenging. Moreover, the flow regimes have not been systematically examined in the case of triangular orifices. Therefore, in the present study, the double emulsion production in planar microfluidic devices with triangle-shaped orifices was observed. The planar microfluidic devices with triangle orifices have several advantages, including the accuracy to fabricate the channel, and the ability to control the local velocity in the channel by modifying the channel design. Thus, we prepared two types of microfluidic devices with orifices and junctions of different shapes, denoted as mc-A and mc-B. The angle of OR1 in mc-B was gentle, which increased the shedding frequency of the emulsion at OR1 and that of the double emulsion at OR2. The junction before OR2 in mc-B was modified to increase the contact area between  $o_{lip}$  and  $w_{ex}$  to stabilize the double emulsion production. As a result, mc-B produced stable double emulsions with a wider range of flow rates and a higher efficiency.

The effects of interfacial tension between  $o_{lip}$  and  $w_{ex}$  on the stable production were examined based on a  $Ca(w_{in} + o_{lip})$  and  $Ca(w_{ex})$  space. The lower interfacial tension increased the area that produced stable double emulsions in the  $Ca(w_{in} + o_{lip})$  and  $Ca(w_{ex})$  spaces in both mc-A and mc-B.

The diameters of the produced emulsions and double emulsions, as indicated by  $D_{in}$  and  $D_{DE}$ , were characterized by a common relationship with exponential indices, which was not influenced by the difference between the microfluidic devices and the external solutions.  $D_{in}$  was characterized as a function of  $Ca(o_{lip})$  and  $Ca(o_{lip})/Ca(w_{in})$ , but  $D_{DE}$  showed a very moderate relationship with  $Ca(w_{ex})$  and  $Ca(w_{ex})/Ca(w_{in} + o_{lip})$ , which indicates that the size of the double emulsions was affected by the size of the small slit of the orifices. However, the stable flow area on a capillary number space to produce stable double emulsions was expanded compared with a device with T-junction or cross-junction.<sup>48</sup>

This study clarified the possibility and limitations of planar microfluidic devices with triangle-shaped orifices. The stable production condition quantified by the capillary number was expanded by modifying the orifice angle to control the local velocities, by widening the cross-junction to cover the discrete phase by increasing the surface area, and by tuning the interfacial tensions. Although  $D_{DE}$  was mainly affected by the orifice size, the obtained double emulsions were highly uniform. The local velocity, which was controlled by the orifice angle, also increases the production efficiency.

#### ACKNOWLEDGMENTS

This study was supported, in part, by a Grant-in-Aid for Scientific Research (B) (Project No. 19H02497) and a Challenging Research (Exploratory) (Project No. 19K22083) from the Japan Society for the Promotion of Science (JSPS KAKENHI)

and by a Fusion-Oriented-Research-for-disruptive-Science-and-Technology (FOREST) from the Japan Science and Technology Agency.

#### DATA AVAILABILITY

The data that support the findings of this study are available from the corresponding author upon reasonable request.

#### REFERENCES

- G. F. Christopher and S. L. Anna, *J. Phys. D: Appl. Phys.* **40**, R319 (2007).
- S.-Y. Teh, R. Lin, L.-H. Hung, and A. P. Lee, *Lab Chip* **8**, 198 (2008).
- C. N. Baroud, F. Gallaire, and R. Danga, *Lab Chip* **10**, 2032 (2010).
- D. Chong, X. Liu, H. Ma, G. Huang, Y. L. Han, X. Cui, J. Yan, and F. Xu, *Microfluid. Nanofluid.* **19**, 1071 (2015).
- S. L. Anna, *Annu. Rev. Fluid Mech.* **48**, 285 (2016).
- L. Shang, Y. Cheng, and Y. Zhao, *Chem. Rev.* **117**, 7964 (2017).
- T. Trantidou, M. S. Friddin, A. Salehi-Reyhani, O. Ces, and Y. Elani, *Lab Chip* **18**, 2488 (2018).
- A. Sattari, P. Hanafizadeh, and M. Hoorfar, *Adv. Colloid Interface Sci.* **282**, 102208 (2020).
- T. Watanabe, I. Motohiro, and T. Ono, *Langmuir* **35**, 2358 (2019).
- N. M. Kovalchuk, E. Roumpea, E. Nowak, M. Chanaud, P. Angeli, and M. J. H. Simmons, *Chem. Eng. Sci.* **176**, 139 (2018).
- S. L. Anna, N. Bontoux, and H. A. Stone, *Appl. Phys. Lett.* **82**, 364 (2003).
- T. Cubaud and T. G. Mason, *Phys. Fluids* **20**, 053302 (2008).
- S. Okushima, T. Nisisako, T. Torii, and T. Higuchi, *Langmuir* **20**, 9905 (2004).
- S. L. Anna and H. C. Mayer, *Phys. Fluids* **18**, 121512 (2006).
- Z. Nie, M. Seo, S. Xu, P. C. Lewis, M. Mok, E. Kumacheva, G. M. Whitesides, P. Garstecki, and H. A. Stone, *Microfluid. Nanofluid.* **5**, 585 (2008).
- W. Lee, L. M. Walker, and S. L. Anna, *Phys. Fluids* **21**, 032103 (2009).
- P. Garstecki, I. Gitlin, W. DiLuzio, G. M. Whitesides, E. Kumacheva, and H. A. Stone, *Appl. Phys. Lett.* **85**, 2649 (2004).
- B. Dollet, W. van Hoeve, J.-P. Raven, P. Marmottant, and M. Versluis, *Phys. Rev. Lett.* **100**, 034504 (2008).
- C. A. Stan, S. K. Y. Tang, and G. M. Whitesides, *Anal. Chem.* **81**, 2399 (2009).
- P. Garstecki, H. A. Stone, and G. M. Whitesides, *Phys. Rev. Lett.* **94**, 164501 (2005).
- P. Garstecki, A. M. Gañán-calvo, and G. M. Whitesides, *Bull. Pol. Acad. Sci.: Tech. Sci.* **53**, 361 (2005).
- W.-L. Ong, J. Hua, B. Zhang, T.-Y. Teo, J. Zhuo, N.-T. Nguyen, N. Ranganathan, and L. Yobas, *Sens. Actuators, A* **138**, 203 (2007).
- Y.-C. Tan, V. Cristini, and A. P. Lee, *Sens. Actuators, B* **114**, 350 (2006).
- D. Funfschilling, H. Debas, H.-Z. Li, and T. G. Mason, *Phys. Rev. E* **80**, 015301(R) (2009).
- K. J. Humphry, A. Ajdari, A. Fernández-Nieves, H. A. Stone, and D. A. Weitz, *Phys. Rev. E* **79**, 056310 (2009).
- T. Fu, Y. Ma, D. Funfschilling, C. Zhu, and H. Z. Li, *AIChE J.* **58**, 3560 (2012).
- T. Fu, Y. Wu, Y. Ma, and H. Z. Li, *Chem. Eng. Sci.* **84**, 207 (2012).
- S. Gulati, K. Vijayakumar, W. W. Good, W. L. Tamayo, A. R. Patel, and X. Niu, *Microfluid. Nanofluid.* **20**, 2 (2016).
- K. Liu, L.-B. Zhao, Q. Zeng, Z.-X. Guo, J. Liu, and X.-Z. Zhao, in *2007 1st International Conference on Bioinformatics Biomedical Engineering* (IEEE, 2007), Vol. 1121, pp. 1121–1124.
- A. R. Abate, A. Poitzsch, Y. Hwang, J. Lee, J. Czerwinski, and D. A. Weitz, *Phys. Rev. E* **80**, 026310 (2009).
- A. S. Utada, E. Lorenceau, D. R. Link, P. D. Kaplan, H. A. Stone, and D. A. Weitz, *Science* **308**, 537 (2005).
- L.-Y. Chu, A. S. Utada, R. K. Shah, J.-W. Kim, and D. A. Weitz, *Angew. Chem., Int. Ed.* **46**, 8970 (2007).
- A. Perro, C. Nicolet, J. Angly, S. Lecommandoux, J.-F. Le Meins, and A. Colin, *Langmuir* **27**, 9034 (2011).

- <sup>34</sup>R. Hidema, T. Oka, Y. Komoda, and H. Suzuki, *Phys. Fluids* **31**, 072005 (2019).
- <sup>35</sup>H. Suzuki, R. Hidema, and Y. Komoda, *Exp. Therm. Fluid Sci.* **67**, 96 (2015).
- <sup>36</sup>Z. Nie, S. Xu, M. Seo, P. C. Lewis, and E. Kumacheva, *J. Am. Chem. Soc.* **127**, 8058 (2005).
- <sup>37</sup>M. Seo, C. Paquet, Z. Nie, S. Xu, and E. Kumacheva, *Soft Matter* **3**, 986 (2007).
- <sup>38</sup>A. R. Abate, J. Thiele, M. Weinhart, and D. A. Weitz, *Lab Chip* **10**, 1774 (2010).
- <sup>39</sup>A. R. Abate, J. Thiele, and D. A. Weitz, *Lab Chip* **11**, 253 (2011).
- <sup>40</sup>S.-Y. Teh, R. Khnouf, H. Fan, and A. P. Lee, *Biomicrofluidics* **5**, 044113 (2011).
- <sup>41</sup>S. C. Kim, D. J. Sukovich, and A. R. Abate, *Lab Chip* **15**, 3163 (2015).
- <sup>42</sup>M. Samandari, F. Alipanaha, S. H. Javanmard, and A. Sanati-Nezhad, *Sens. Actuators, B* **291**, 418 (2019).
- <sup>43</sup>M. J. Jensen, H. A. Stone, and H. Bruus, *Phys. Fluids* **18**, 077103 (2006).
- <sup>44</sup>C. Zhou, P. Yue, and J. J. Feng, *Phys. Fluids* **18**, 092105 (2006).
- <sup>45</sup>Y. Chen, L. Wu, and L. Zhang, *Int. J. Heat Mass Transfer* **82**, 42 (2015).
- <sup>46</sup>S. A. Nabavi, S. Gu, G. T. Vladislavljević, and E. E. Ekanem, *J. Colloid Interface Sci.* **450**, 279 (2015).
- <sup>47</sup>M. Azarmanesh, M. Farhadi, and P. Azizian, *Phys. Fluids* **28**, 032005 (2016).
- <sup>48</sup>N. Wang, C. Semperebon, H. Liu, C. Zhang, and H. Kusumaatmaja, *J. Fluid Mech.* **895**, A22 (2020).
- <sup>49</sup>S. Tan, C. Gao, H. Liu, B. Ye, and D. Sun, *Colloids Surf., A* **601**, 124917 (2020).
- <sup>50</sup>W. Yu, X. Liu, Y. Zhao, and Y. Chen, *Chem. Eng. Sci.* **203**, 259 (2019).
- <sup>51</sup>M. Noorandooost, M. Haghshenas, M. Muradoglu, and R. Kumar, *Microfluid. Nanofluid.* **23**, 31 (2019).